EFFICIENCY OF GROUND MOTION INTENSITY MEASURES WITH EARTHQUAKE-INDUCED EARTH DAM DEFORMATIONS

Richard J. Armstrong[1], Tadahiro Kishida[2], and DongSoon Park[3]

[1] California State University, Sacramento, United States.
[2] Khalifa University, United Arab Emirates.
[3] K-Water Convergence Research Institute, Republic of Korea.

Abstract

In a seismic hazard analysis (SHA), the earthquake loading level should be predicted for one or more ground motion intensity measures (IMs) that are expected to relate well with the engineering demand parameters (EDPs) of the site. In this particular study, the goal was to determine the IMs that best relate to embankment dam deformations based on non-linear deformation analysis (NDA) results of two embankment dams with a large suite of recorded ground motions. The measure utilized to determine the "best" IM was standard deviation in the engineering demand parameter (e.g., deformation) for a given IM—$\sigma_{\ln EDP|\ln IM}$, also termed "efficiency." Results of the study demonstrated that for the NDA model used, Arias intensity (AI) was found to be the most efficient predictor of embankment dam deformations. In terms of spectral acceleration (SA)-based IMs, the SA at short periods and then in the general range of the natural period of the dams were seen to be the most efficient IM, but was in almost all cases not as efficient as AI. In terms of total standard deviation ($\sigma_{\ln DYF|M,R,S}$) of EDP conditioned on earthquake source parameters, the poor predictability of AI relative to other IMs resulted in a higher total standard deviation given an earthquake. Within this context, CAV was deemed the best IM.

Introduction

In a seismic evaluation of an embankment dam, the earthquake loading level should be predicted for one or more ground motion intensity measures (IMs) that are expected to relate well with the engineering demand parameters (EDPs) of the site. For embankment dams, the EDP of interest is typically horizontal or vertical crest displacement, and the IMs often selected are spectral acceleration (SA), peak ground velocity (PGV), and Arias intensity (AI). The design target level for one or more of these IMs is then predicted as part of a seismic hazard analysis. In dam engineering practice in the United States, deterministic seismic hazard analyses are still very common. In conducting these deterministic seismic hazard analyses, the conventional approach for setting the design target levels is to select the target value of each intensity measure to represent a specified percentile level uniformly. An alternative to this approach is to select a single intensity measure, called the conditioning intensity measure, that relates well to embankment-dam response and then to apply this percentile level to that particular intensity measure only. The mean values of the other intensity measure targets are then selected, given (or "conditioned on") the value of the conditioning intensity measure. The second approach is

termed the conditional mean approach. A comparison of the conventional and conditional mean approaches in the context of dam-engineering practice is found in Armstrong (2017).

In a seismic hazard analysis, an important consideration is which IMs are to be used. This especially in the case with selecting the conditioning intensity measure, because the hazard level most directly relates to this IM. An optimal type of IM should relate well to the EDP of interest—in the case of dams, for example, horizontal or vertical crest displacement. Determination of such an "optimal" IM has been previously related to the so-called efficiency and sufficiency of the IM (Cornell and Luco, 2001). Efficiency is related to the variability in the random error term in the regression analysis between the $\ln IM$ and the $\ln EDP$ ($\sigma_{\ln EDP|\ln IM}$). In this context, IMs that produce less $\sigma_{\ln EDP|\ln IM}$ in predicting EDP are considered more efficient. The term sufficiency relates to the ability of an IM to predict the EDP without the need for specifying the earthquake magnitude or site-to-source distance. In this context, a sufficient IM would have a random error term from the regression analysis that did not demonstrate any bias with magnitude and site-to-source distance.

The efficiency of IMs in the context of embankment and slope deformations has been investigated in previous studies (e.g., Bray and Travasarou, 2007; Saygili and Rathje, 2007; and Beaty and Perlea, 2012). Based on these studies, it has been suggested that for stiff embankment dams in which significant strength loss is not expected, the SA at the first-mode period of the structure relates well with embankment deformations. However, for embankment dams founded on liquefiable alluvium, other non-SA intensity measures have been found to relate better to embankment deformations (Beaty and Perlea, 2012)—such as AI; cumulative absolute velocity, CAV; and $\sqrt{AI \cdot D595}$, where $D595$ is the duration between 5% and 95% AI. These studies, however, have been based on either Newmark-type sliding block analyses with large ground motion databases (e.g., Bray and Travasarou, 2007; Saygili and Rathje, 2007) or on non-linear deformation analyses shaken with significantly smaller sets of ground motions (Beaty and Perlea, 2012).

In this study—supported by the California Department of Conservation, California Geological Survey, Strong Motion Instrumentation Program, Agreement 1016-988—data from strong ground motion recordings during the 1989 Loma Prieta earthquake were used to validate non-linear deformation analysis models of Lenihan and Anderson dams that were subsequently used in assessing the efficiency of ground motion IMs with embankment-dam deformations. A suite of 342 recorded ground motions were used with these validated NDA models to assess the relationship between ground-motion characteristics and embankment-dam deformations. The paper begins with a summary of the NDA of Lenihan and Anderson dams during the 1989 Loma Prieta earthquake. Subsequently, the ground motion database used in the analysis is described, followed by presentation of the results in the context of the efficiency of each IM. The impacts of including the predictability of each IM in predicting deformations are also discussed. The paper ends with conclusions from this study.

NDA Validation Against 1989 Loma Prieta Earthquake

Description of Embankment Dams

James J. Lenihan Dam is a 207-ft-high zoned earthfill dam that was constructed in 1952 (Figure 1). Lenihan Dam impounds a reservoir that has a maximum capacity of 19,044 acre-ft at the spillway elevation of 653 ft (TGP, 2012). The zoned earthfill dam is composed of upstream and downstream shells, core, and drainage zones. The core is further divided into an upper and lower core to reflect differences in material properties. The upstream shell is composed of gravelly clayey sands to sandy clays, while the upper core is composed of gravelly clayey sand to clayey gravel. The lower core is classified as highly plastic sandy clays to highly plastic silty sands-sandy silts. The downstream shell consists of gravelly clayey sand to clayey gravels. The embankment materials were constructed on Franciscan Complex bedrock, without a foundation seepage cutoff or grout curtain. Instrumentation at this dam includes survey monuments, piezometers, inclinometers, seepage weir, and strong ground motion instruments.

A new seismic evaluation of Lenihan Dam was performed in 2011 by Terra-GeoPentech (TGP, 2012) and reviewed by Division of Safety of Dams (DSOD) (Kuhl, 2012). This new study included a site investigation, site characterization, and subsequent deformation analyses. Important outcomes were: (1) no alluvium or colluvial soils were left in place beneath the embankment; (2) no liquefiable materials were located within the dam or the dam foundation, (3) all embankment materials were well-compacted (with the exception of the internal drainage zones); and (4) for the design earthquake, no seismic remedial measures are necessary.

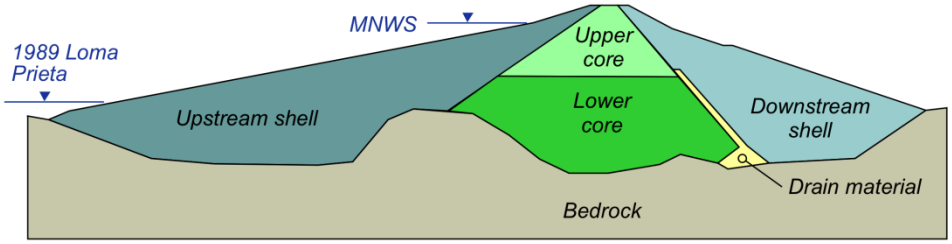

Figure 1: Design cross-section with reservoir level of 556 ft during the 1989 Loma Prieta Earthquake and at the maximum normal water surface elevation of 653 ft.

Anderson Dam is a 240-ft-high zoned rockfill and earthfill embankment (Figure 2). The dam was originally constructed to an elevation of 641 ft in 1950; it was subsequently raised to an elevation of 647.2 ft in 1987. Anderson Dam impounds a reservoir that has a maximum capacity of 90,000 acre-ft at the spillway elevation of 627.8 ft (Ryan et al., 2013). The zoned dam includes upstream and downstream rockfill shells, a compacted clay core, and a graded transition between the rockfill and clay core (Ryan et al., 2013). The rockfill shells are composed of cobbles and gravel with varying amounts of sand and clay, and the clay core is composed of clayey sand with gravel and sandy clay with gravel. The finer rockfill found within the lower portions of the shells (named lower finer fill, or LFF) is composed of clayey sand with gravel. The foundation alluvium ranges from clayey gravel with sand to clayey sand with gravel.

Bedrock is composed of Franciscan Melange. Instrumentation includes survey monuments, piezometers, inclinometers, and strong ground motion instruments.

A new seismic evaluation study of Anderson Dam occurred in 2011 by AMEC Geomatrix (AMEC, 2011) and review by DSOD (Dorsey, 2011). This new study included a detailed site investigation program, site characterization, and subsequent deformation analyses. Important outcomes of this study were: (1) the alluvium, primarily clayey sand with gravel; was susceptible to liquefaction; (2) the lower finer fill (LFF) was also susceptible to liquefaction, and (3) the cyclic resistance estimated from Becker Hammer Penetration testing (BPT) was less than the anticipated cyclic stress demand, so liquefaction triggering and shear strength loss were expected to occur. As a result of liquefaction in the lower finer fill and alluvium, large earthquake-induced deformations were expected by both AMEC and DSOD (Dorsey, 2011). As a result, a significant reservoir restriction was imposed, and a seismic remediation is currently planned.

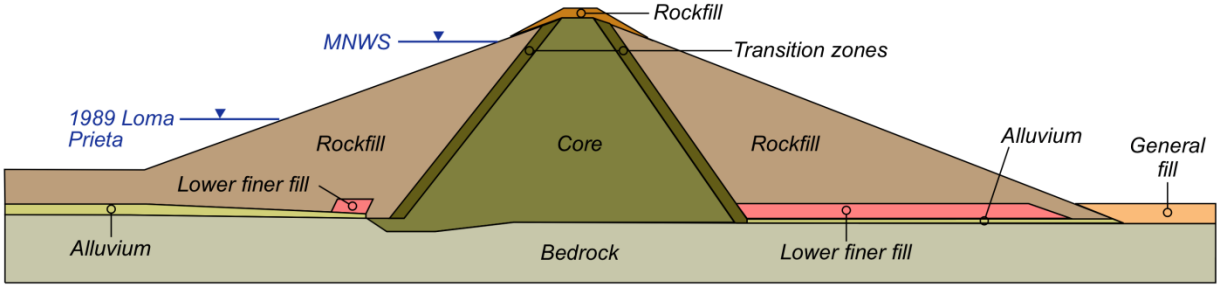

Figure 2: Design cross-section of Anderson Dam with reservoir level of 513 ft during the 1989 Loma Prieta Earthquake and at the MNWS elevation of 628 ft.

Numerical Analysis Details

The response of each dam in the 1989 Loma Prieta earthquake was modeled with non-linear deformation analyses (NDA) using the program FLAC (Itasca Consulting Group, 2016). This program uses an explicit solution scheme and is well suited for performing deformation analyses with non-linear material response, large geometry changes, and instability. The numerical meshes used in the NDA of Lenihan and Anderson Dams are shown in Figures 3 and 4, respectively. The element sizes of each model ranged from around 2 ft to 10 ft and were able to transmit motion frequencies accurately up to at least 10 hertz.

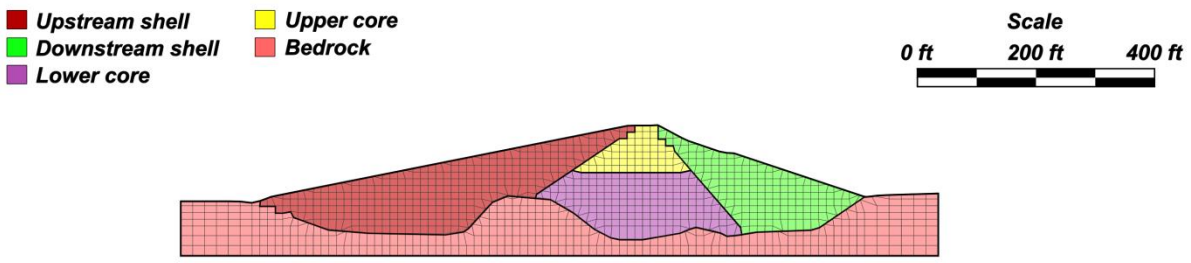

Figure 3: Numerical mesh for Lenihan Dam.

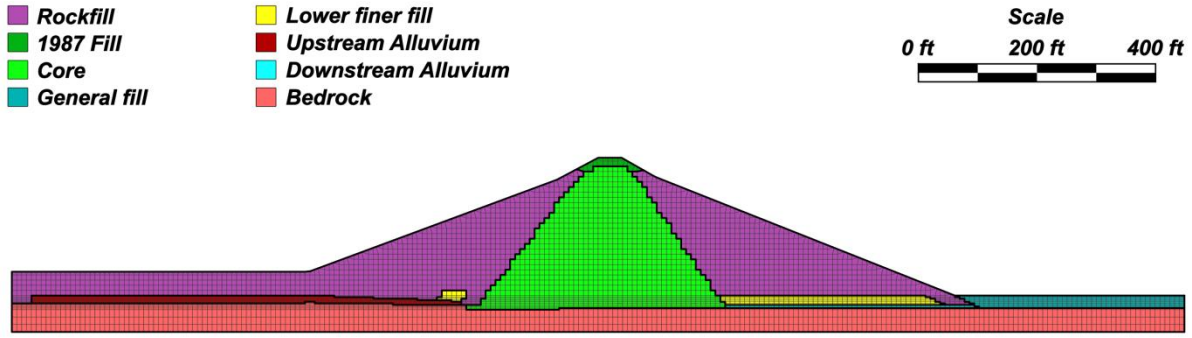

Figure 4: Numerical mesh for Anderson Dam.

Characterization of Material Properties

The expected non-linear soil response in the embankment and soil foundation was modeled in FLAC using either the UBCHYST or PM4Sand constitutive models. The UBCHYST constitutive model (Byrne and Naesgaard, 2015) was utilized for all soils in which the dynamic response could be modeled either as fully-drained or undrained and without significant strength-loss during shaking. For coarse-grained soils in which changes in excess porewater pressure during shaking were deemed critical to capture, the PM4Sand model (Boulanger and Ziotopoulou, 2017) was utilized. The calibration protocol utilized for UBHYST is described in Armstrong (2018a) and the calibration protocol for PM4Sand in Armstrong (2018b). The material properties recommended from recent studies (AMEC, 2011 and TGP, 2012) were either used directly in the NDA or modified based on alternative assumptions. All material properties used in these analyses are provided in Armstrong (2008c).

Establishment of Pre-Earthquake Stresses and Boundary Conditions

The state of stress was modeled prior to the earthquake, because these stresses affect both the initial conditions for the dynamic analysis and the values of shear strength. Total stresses for the embankment were estimated by sequentially adding rows of elements of the mesh and solving for static equilibrium with each new row of elements. This process was continued for the entire embankment. The goal of this process was to mimic roughly the actual construction process. Porewater pressures were based on a seepage analysis of each dam prior to the 1989 Loma Prieta earthquake. Note that prior to the 1989 Loma Prieta earthquake, less-than-average rainfall had occurred for several years, and both reservoirs were low relative to the normal. For Lenihan Dam, the reservoir was at 556 ft, significantly below the maximum normal water surface (MNWS) elevation of 653 ft; and for Anderson Dam, the reservoir was 513 ft, also significantly below the MNWS elevation of 628 ft. For these non-steady state seepage conditions, the approach used for modeling was threefold: (1) to capture first the steady-state seepage conditions corresponding to the MNWS, (2) to change the boundary conditions to model the lower reservoir level during the earthquake, (3) to rerun the analysis until the porewater pressure in the embankment was lowered to the values similar to those measured prior to the 1989 Loma Prieta earthquake. For the initial steady-state seepage conditions corresponding to the reservoir at the MNWS, the horizontal and vertical permeabilities were adjusted until the

calculated total head reasonably corresponded to piezometer recordings when the reservoir was near the same elevation.

Dynamic Analysis Results

Strong ground motion recordings from the 1989 Loma Prieta earthquake were utilized in the NDAs in two ways: (1) as a direct input at the base of each NDA, and (2) as a comparison to the calculated time histories from the NDAs. Three strong ground motion instruments were available at Lenihan Dam: a strong ground motion instrument located on the left abutment and two instruments located along the embankment crest. Eight strong ground motion instruments were available at Anderson Dam: a strong ground motion instrument located at the left abutment, two instruments at the toe and downstream of the embankment, three instruments located along the crest, and two instruments along the downstream slope.

The ground motion used as the input at the base of the NDA for Lenihan Dam corresponded to the abutment strong ground motion recording in the transverse direction. For Anderson Dam, the ground motion input at the base of the NDA was the toe strong ground motion recording in the transverse direction. The toe recording at Anderson Dam was used because it resulted in the calculated crest response in the NDA much more similar to that observed than when the abutment recording was used as the input at the base of the NDA. The velocity time histories of the strong ground motion recordings (i.e., abutment recording for Lenihan Dam and toe recording for Anderson Dam) were converted to shear stress time histories and applied to the base of the numerical model. The "field-field" condition used in FLAC was applied along the vertical boundary of the foundation soil and rock, and numerical dashpots were applied along the vertical foundation soil and rock and along the base of the numerical model.

As an initial evaluation of the NDA results, the IMs calculated from the NDA are compared to those measured from similarly located strong motion recordings (Figures 5 and 6). In particular, for Lenihan Dam, SA calculated from the crest is compared to the SA measured from the two strong motion recordings located along the crest. For Anderson Dam, SA calculated at the crest is compared to the SA measured from a strong ground motion recording located along the approximate maximum section of the dam. The calculated ratio of the SA from the crest to the SA from the base (termed RSA) of the NDA is also compared to that measured in Figures 5 and 6. For Lenihan Dam, the measured values of RSA correspond to the ratio of the SA from the crest at either of the two strong motion recordings at the crest (i.e., SA_i with i = Lt. crest or Rt. crest) to the SA from the strong ground motion recording at the rock abutment. For Anderson Dam, the measured values of RSA correspond to the ratio of the SA from the crest at the strong ground motion recording located along the approximate maximum section of the dam to the SA from the strong ground motion recording at the toe or abutment (e.g., SA_i with i = Toe or Abutment). Finally, in Figures 5 and 6, PGV, AI, and $D595$ are computed at the crest from the NDA and compared to those measured from the same strong ground motion recordings at the crest as used in determining the crest SA.

As seen in Figures 5 and 6, the general trends and magnitude of IMs were captured reasonably well with the NDA. For Lenihan Dam, computed crest PGA, PGV, and AI were 17.6%, 2.5%, and 19.2% smaller, respectively, than measured from the left crest strong ground motion recording. PGA, PGV, and AI were 30.0%, 13.8%, and 52.2% smaller, respectively, than

measured from the right crest strong ground motion recording. $D595$ was computed 61.8% (left crest instrument) and 43.2% (right crest instrument) larger than that measured. For Anderson Dam, the computed crest PGA, PGV, and AI were 35.2%, 24.3%, and 37.9% smaller than the measured values, respectively, with $D595$ computed 1.9% larger than that measured.

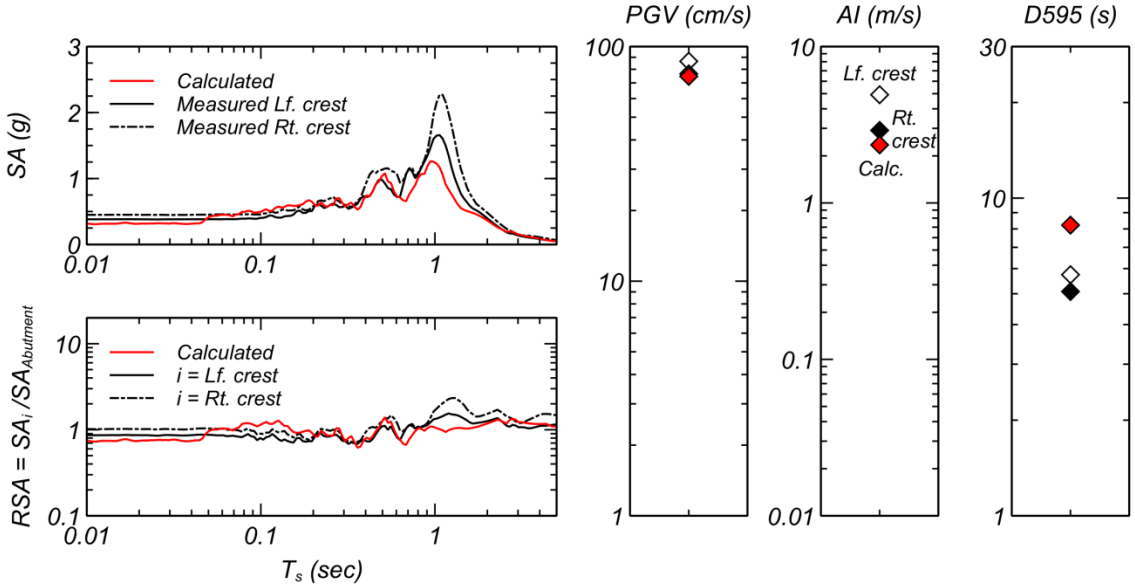

Figure 5: Summary of the calculated and measured dynamic responses for Lenihan Dam.

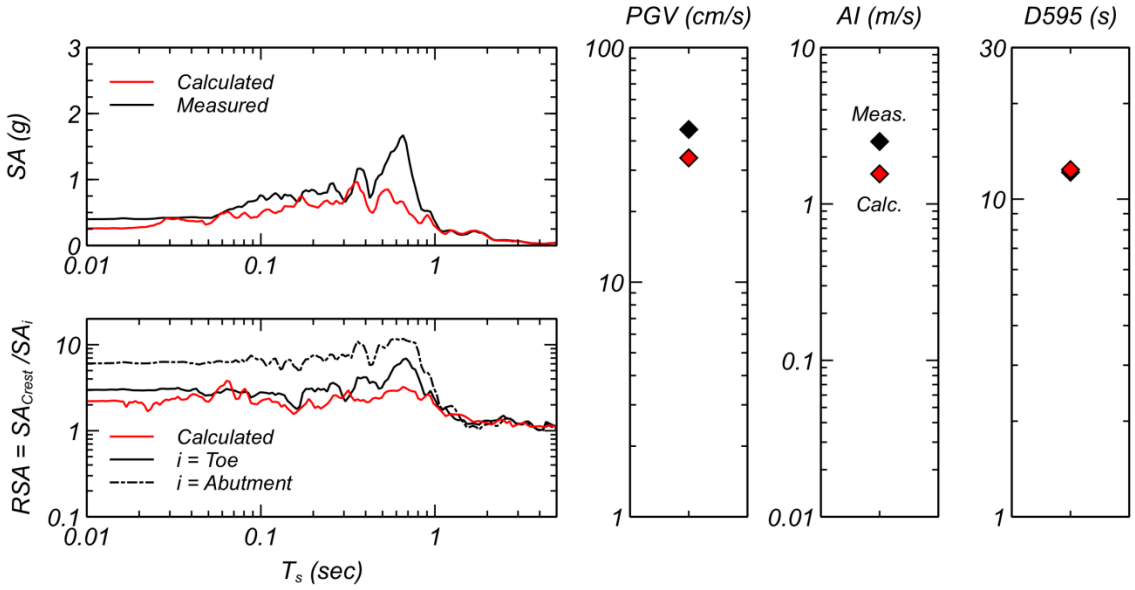

Figure 6: Summary of the calculated and measured dynamic responses for Anderson Dam.

In terms of SA, the periods in which the largest amplifications were observed (i.e., local maximums in RSA) were generally captured, but these magnitudes were less than those observed. For Lenihan Dam, the local maximum of RSA at T_s = 0.52 sec was observed at both

crest strong ground motion records, and was well captured by the NDA. However, the other local maximums of RSA at 1.2 sec or 1.3 sec were underpredicted by this NDA. For Anderson Dam, RSA was significantly underpredicted for T_s = 0.66 s, regardless if RSA was computed from the abutment or toe recording.

Computed final crest displacement in the horizontal direction (DXF, positive downstream) and vertical direction (DYF, positive downward) are summarized in Table 1 with comparison to those measured. As highlighted in Table 1, the displacements computed were in the general range of those measured.

Table 1. Comparison of computed and measured crest deformations.

	DXF	DYF
Lenihan Dam		
Measured	0.10 – 0.25 ft	0.61 – 0.85 ft
Calculated	0.42 ft	0.75 ft
Anderson Dam		
Measured	Negligible	0.04 – 0.13 ft
Calculated	-0.02 ft	0.34 ft

Numerical Analysis Ground Motion Study

Characteristics of Ground Motion Database

The ground motion database used in this study was composed of recordings with: (1) distance R_{rup} less than 30 km, similar to many dams in California; (2) magnitude $M_w \geq 5$, because it was expected that ground motions would produce appreciable deformations; and (3) $AI \geq 1$ m/s to further reduce the ground motion considered and ensure appreciable deformations. Initially, the ground motion database used in this study was composed of a subset similar to the NGA West 1 ground motion recordings (Chiou et al., 2008) as used by Armstrong (2016). The database used in the ground motion study was later augmented with new ground motion recordings from the NGA West 2 database (Ancheta et al., 2014), as well as those from the NGA West 1 database that had not been included in the initial ground motion study but that satisfied the selection criteria. In total, 342 single-component ground motions were used in the ground motion study; for those ground motions, the distribution of M_w, R_{rup}, and fault mechanisms are shown in Figure 7.

The 342 single-component ground motions represent 48 different earthquake events. The list of event names and the number of single-component ground motions utilized are summarized in Table 2. The five most frequent events in which ground motions were used are (in descending order, with percent of total included): (1) 1999 Chi-Chi Taiwan, 23.1%; (2) 1994 Northridge-01, 17.5%; (3 and 4) 1970 Imperial Valley-06 and 1989 Loma Prieta, 7.9%; and (5) 1995 Kobe Japan, 2.9%. The other 43 events account for the remaining 40.6% of ground motions.

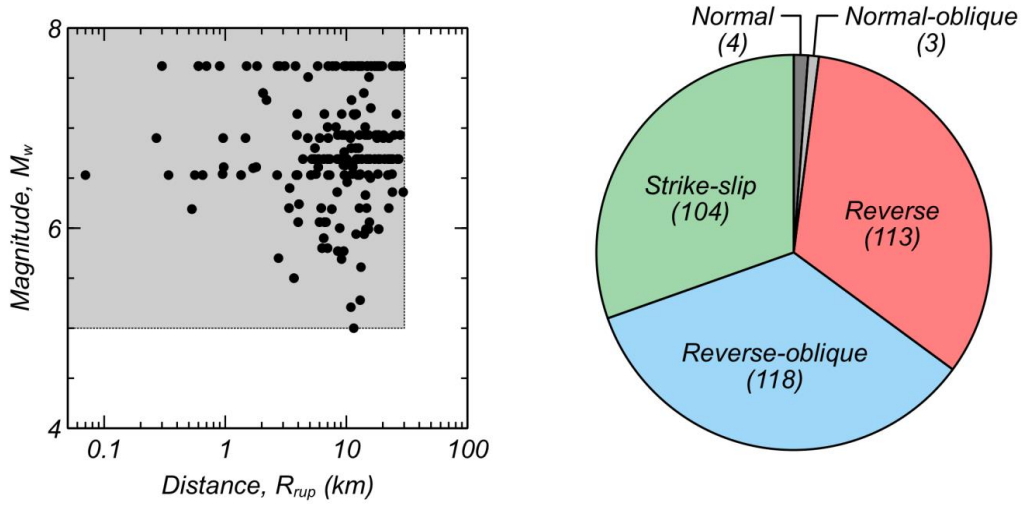

Figure 7: Range of M_w, R_{rup}, and fault mechanisms used in ground motion study.

Table 2. Distribution of earthquake events of ground motion study.

Event	Ground motions	Event	Ground motions
1970 Imperial Valley-06	27	1990 Mammoth Lakes-04	1
1971 San Fernando	2	1991 Sierra Madre	1
1972 Managua Nicaragua-01	2	1992 Big Bear-01	2
1976 Friuli Italy-01	1	1992 Cape Mendocino	6
1976 Gazi USSR	2	1992 Landers	4
1978 Tabas, Iran	4	1994 Northridge-01	60
1980 Irpinia, Italy-01	2	1994 Northridge-06	1
1980 Mammoth Lake-01	4	1995 Dinar Turkey	2
1980 Mammoth Lakes-02	1	1995 Kobe, Japan	10
1980 Mammoth Lakes-06	3	1999 Chi-Chi, Taiwan	79
1980 Victoria, Mexico	2	1999 Chi-Chi, Taiwan-03	3
1981 Wetmorland	2	1999 Chi-Chi, Taiwan-04	2
1983 Coalinga-01	4	1999 Duzce, Turkey	9
1983 Coalinga-05	4	1999 Hector Mine	1
1983 Coalinga-07	1	1999 Kocaeli, Turkey	4
1984 Morgan Hill	2	2000 Tottori, Japan	6
1985 Nahanni, Canada	2	2000 Yountville	1
1986 Chalfant Valley	2	2003 Bam, Iran	2
1986 N. Palm Springs	4	2004 Niigata, Japan	8
1986 San Salvador	4	2004 Parkfield-02	2
1987 Baja California	2	2007 Chuetsu-oki, Japan	8
1987 Supersition Hills-02	9	2008 Iwate, Japan	8
1987 Whittier Narrows-01	5	2010 El Mayor-Cucapah, MX	2
1989 Loma Prieta	27	2011 Christchurch	2

Similar to the 1989 Loma Prieta earthquake analysis, the velocity time histories of the 342 ground motion recordings were converted to shear stress time histories, which were then inputted at the base of the NDAs. The IMs for the resulting time histories at the base of the NDAs are shown in Figure 8 in terms of PGA, PGV, AI, CAV, and $D595$. Differences between IMs calculated from Lenihan and Anderson dams are due to ground motions being inputted as shear stress time histories; therefore, the calculated acceleration time history is a function of the shear stress time history as well as the overall response of the NDA model.

Referencing the base motion from the NDA from the 1989 Loma Prieta earthquake, it is seen that for Lenihan Dam, ground motions in this database have IMs that extend from less than to greater than the IMs from the 1989 Loma Prieta earthquake. For Anderson Dam, the ground motions in the database had IMs much greater than the 1989 Loma Prieta earthquake. For both dam NDA models, therefore, it is expected that the resulting deformations will go from negligible to values greater than those calculated with the 1989 Loma Prieta earthquake.

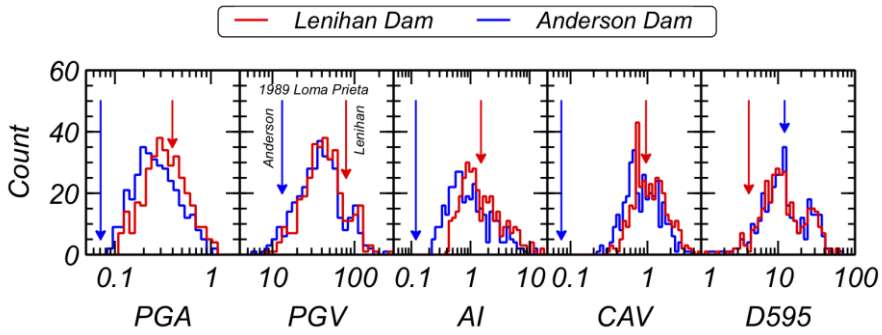

Figure 8: Distribution of IMs of ground motion recordings in study. Red and blue arrows correspond to the IM levels for Lenihan and Anderson dams, respectively, during the 1989 Loma Prieta earthquake.

Numerical Analysis Results

Overview

Analyses of the NDA models of Lenihan and Anderson dams were conducted with the 342 ground motion time histories described above. The NDA models used were identical to those used in the 1989 Loma Prieta analyses, except that the reservoir level used now corresponded to the MNWS elevations. For each analysis, time histories at key locations were stored, as well as the final solved state of the NDA model. Summary of key statistical metrics are provided in Table 3 for $IM = PGA$, PGV, AI, CAV, and $D595$ at the base and crest of the NDA models, as well as DXF and DYF (i.e., horizontal and vertical crest displacements). Ranges of IMs are significant, as are the displacements. Displacements ranged from negligible to values comparable to or greater than those computed in recent seismic evaluation studies by AMEC (2011), Dorsey (2011), TGP (2011), and Kuhl (2012).

Regression Analysis

Utilizing the results from the NDA ground motion study, the relationship between ground motion characteristics and embankment dam deformations of the two NDA models was assessed through single-variate, least-squares regression analyses between ln IMs and ln EDPs. The IMs considered were the base and crest PGA, PGV, AI, CAV, and $D595$, and the SA and RSA at 200 equal logarithmic increments of spectral period (T_s) between 0.01 and 10 seconds. PGA is taken as SA at T_s = 0.01 s. The EDPs considered were the peak and final horizontal displacements (DXP and DXF) and the peak and final vertical displacements (DYP and DYF). With the 204 IMs at the crest and base and 4 EDPs, a total of 1,632 least-squares linear regression analyses were conducted. In evaluating the regression analyses, the efficiency in EDP given each IM (i.e., $\sigma_{\ln EDP|\ln IM}$) was computed from the 1,632 least-squares linear regression analyses.

Table 3. Summary statistics from NDA study.

Item		Lenihan Dam			Anderson Dam		
		Geometric mean	MIN	MAX	Geometric mean	MIN	MAX
Base	PGA (g)	0.33	0.11	1.13	0.27	0.09	1.16
	PGV (cm/s)	42.57	9.78	263.66	37.31	6.18	259.05
	AI (m/s)	1.52	0.42	17.07	0.97	0.24	12.35
	CAV (g·sec)	1.07	0.31	4.57	0.86	0.24	3.58
	$D595$ (sec)	11.66	0.88	62.10	11.75	1.24	67.16
Crest	PGA (g)	0.33	0.17	0.50	0.33	0.18	0.61
	PGV (cm/s)	51.87	18.03	277.40	54.46	21.54	283.32
	AI (m/s)	3.35	0.74	13.38	4.10	0.89	13.66
	CAV (g·sec)	1.99	0.51	7.69	2.20	0.66	7.49
	$D595$ (sec)	19.37	3.70	249.02	18.30	3.36	249.76
	DXF (ft)	0.87	0.03	8.89	0.45	0.004	5.29
	DYF (ft)	0.63	0.06	5.31	3.14	0.53	26.10

Scatter plots of $EDP = DXP$, DXF, DYP, and DYF versus $IM = PGA$, PGV, AI, CAV, and $D595$ are shown in Figure 9 for the NDA model of Lenihan Dam and in Figure 10 for the NDA model of Anderson Dam. Note that for each plot, the horizontal and vertical axes are logarithmic, with the range equal to the minimum and maximum values in Table 3. The least-squares linear regression lines (solid red line) and 1 standard deviation ($\sigma_{\ln EDP|\ln IM}$) above and below the regression lines (dotted red lines) are also included for reference. IMs in the figures were calculated at the base of numerical models. The standard deviation computed from each of the regression analyses in Figures 9 and 10 are provided in Table 4.

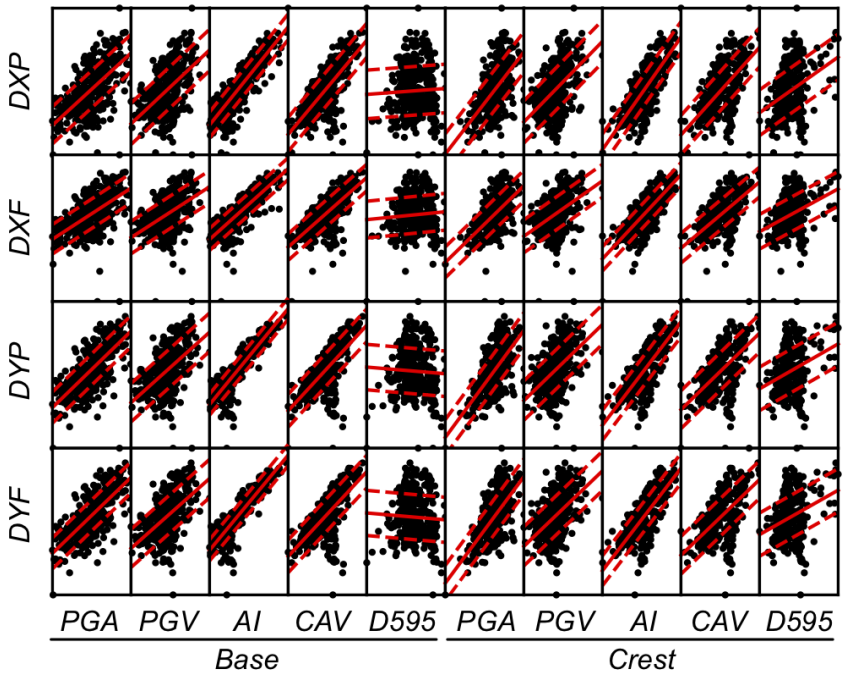

Figure 9: Comparison of IMs and EDPs for model of Lenihan Dam (all axes are logarithmic).

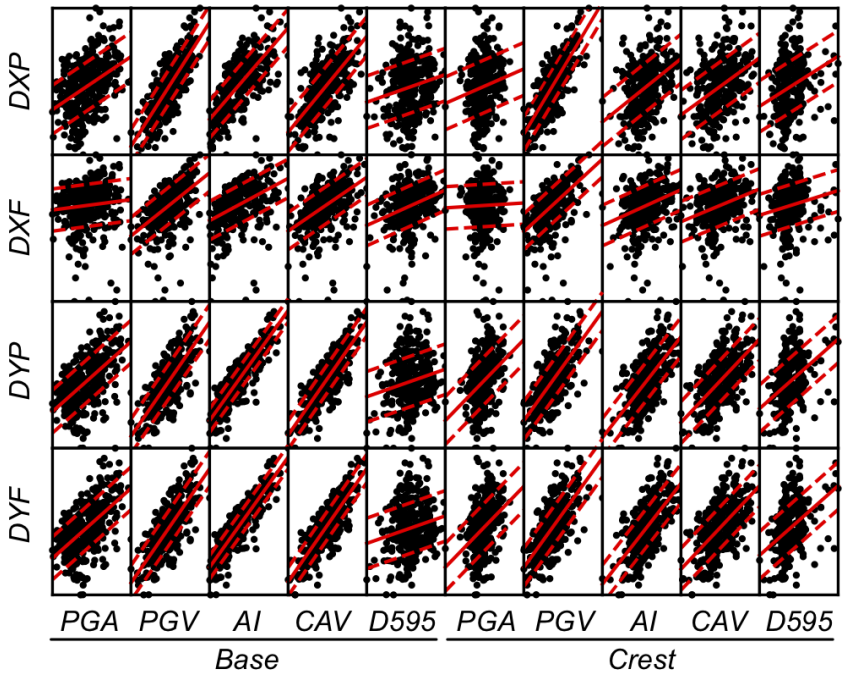

Figure 10: Comparison of IMs and EDPs for model of Anderson Dam (all axes are logarithmic).

Table 4. $\sigma_{\ln EDP|\ln IM}$ from regression analysis for models of Lenihan and Anderson dams.

IM	Lenihan Dam				Anderson Dam			
	DXP	DXF	DYP	DYF	DXP	DXF	DYP	DYF
Base								
PGA	0.517	0.572	0.478	0.480	0.653	1.026	0.568	0.569
PGV	0.574	0.629	0.588	0.592	0.454	0.897	0.461	0.461
AI	0.359	0.424	0.324	0.328	0.501	0.939	0.312	0.312
CAV	0.474	0.515	0.503	0.507	0.522	0.904	0.375	0.375
$D595$	0.674	0.714	0.695	0.699	0.703	0.988	0.671	0.672
Crest								
PGA	0.562	0.599	0.546	0.549	0.706	1.031	0.635	0.635
PGV	0.586	0.639	0.603	0.607	0.450	0.870	0.508	0.508
AI	0.434	0.469	0.458	0.462	0.655	0.989	0.512	0.512
CAV	0.543	0.576	0.579	0.584	0.660	0.991	0.556	0.556
$D595$	0.635	0.671	0.665	0.670	0.688	1.017	0.630	0.630

In evaluating the results of Figures 9 and 10 and Table 4, it can be seen that AI at the base of the model was in almost all cases the most efficient predictor (i.e., lowest $\sigma_{\ln EDP|\ln IM}$). Following AI, CAV was typically the most efficient predictor. Note that the one exception in the previous ranking was DXF for the NDA model of Anderson Dam in which PGV was actually slightly more efficient, with $\sigma_{\ln DXF|\ln PGV}$ = 0.897. In fact, for Anderson Dam, the IMs considered were not able to predict DXF as efficiently with DYF.

In terms of SA-based IMs, $\sigma_{\ln EDP|\ln IM}$ was also computed for $EDP = DXF$ and DYF against SA at the base of the numerical models. Figures 11 and 12 show the distribution of $\sigma_{\ln EDP|\ln IM}$ with spectral period for both dams. These figures also show for comparison $\sigma_{\ln EDP|\ln IM}$ for $IM = PGV$, AI, and CAV at the base of the numerical models. Note that the trends observed in $\sigma_{\ln EDP|\ln IM}$ for SA at the base of the NDA models were similar to $\sigma_{\ln EDP|\ln IM}$ with SA corresponding to the crest and with the ratio of the SA at the crest to SA at the base SA (i.e., RSA).

The efficiency of SA at the base of the numerical model was strongly dependent on the spectral period, T_s. Also, two local minima with the lowest $\sigma_{\ln EDP|\ln IM}$ (highest efficiency) were observed: (1) very low T_s (e.g., the PGA) and (2) T_s in the range of 0.3 to 0.6 seconds for Lenihan Dam and $T_s \approx 1$ second for Anderson Dam. The second local minimum represents roughly the natural period of the dam. The natural period of the dam would differ depending on the degree of soil non-linearity exhibited, but it is noted that the natural periods in which these minimums are observed are similar to the same models shaken with the 1989 Loma Prieta earthquake (i.e., Figures 5 and 6).

In this study, although SA at a T_s near the natural period of the dam demonstrated the highest efficiency for SA-based IMs, a non-SA based IM, AI at the base (i.e., the rock foundation

condition), was in fact the most efficient IM considered with the only exception being DXF for the NDA model of Anderson Dam. It is important to note that this observation is true for two dams with differing responses: one with liquefaction (Anderson Dam), and the other without liquefaction (Lenihan Dam). In the latter case, with an embankment without liquefaction, conventional understanding (e.g., Bray and Travasarou, 2007) would suggest that SA at the natural period of the dam should relate best to deformations; however, for these two dam models analyzed with NDAs, this is not the case.

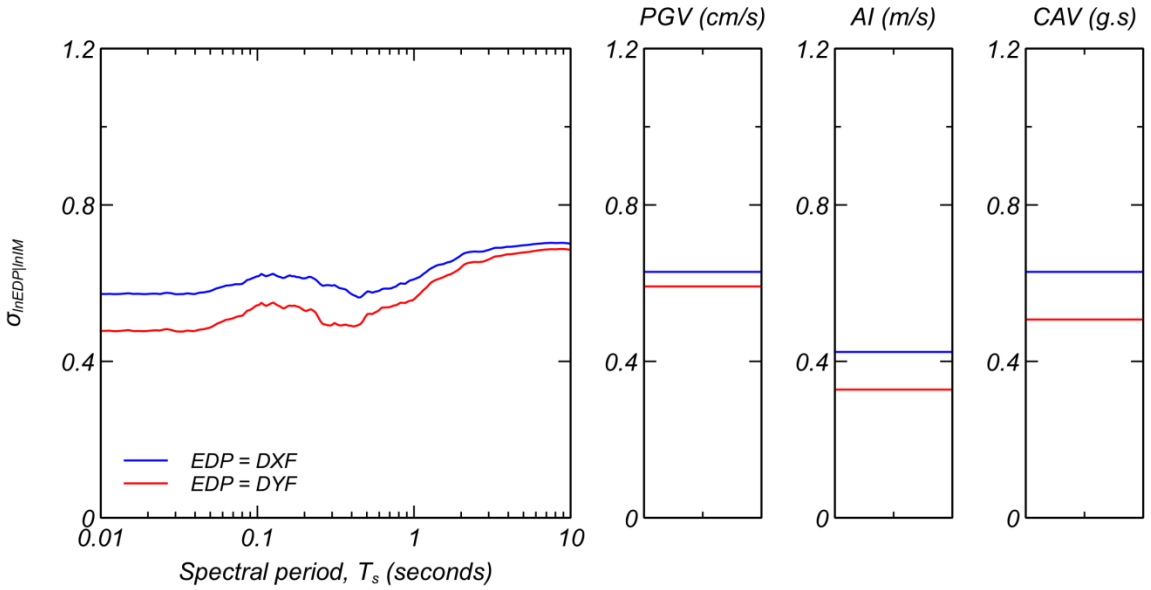

Figure 11: $\sigma_{\ln EDP|\ln IM}$ for SA, PGV, AI, and CAV for the NDA model of Lenihan Dam.

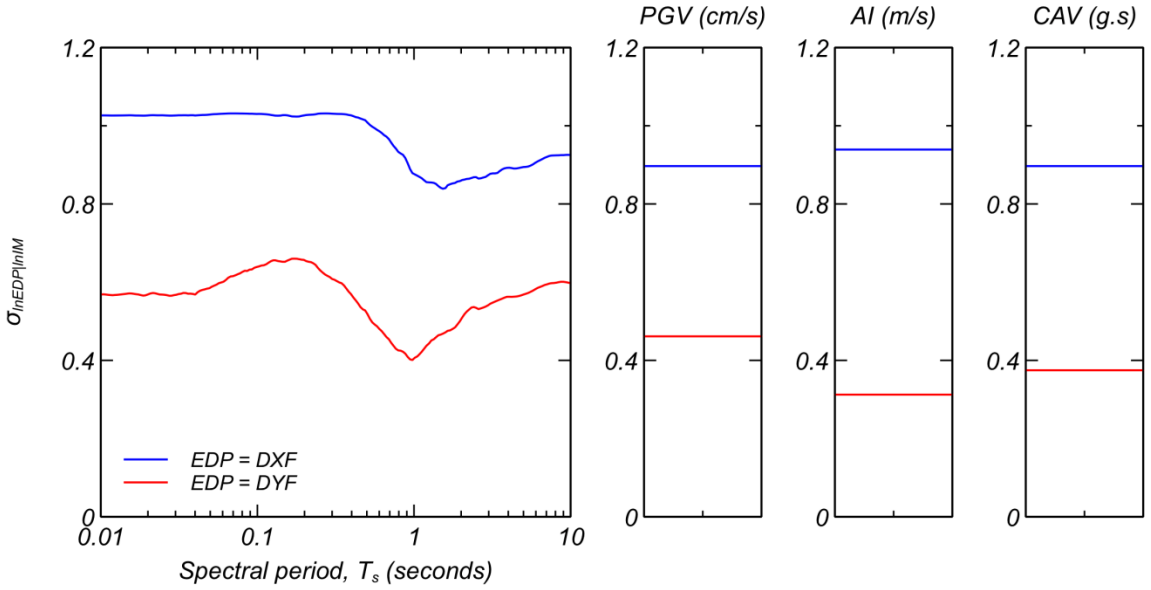

Figure 12: $\sigma_{\ln EDP|\ln IM}$ for SA, PGV, AI, and CAV for the NDA model of Anderson Dam.

Discussion

Although the efficiency accounts for the uncertainty in EDP for a given IM, it does not account for the uncertainty in the IM when predicted for a specific earthquake scenario. This uncertainty—termed predictability ($\sigma_{\ln IM|M,R,S}$)—is estimated through common ground motion prediction equations (GMPE) and is a function of the earthquake magnitude (M), the source-to-site distance (R), and other site conditions (S). The predictability defers for each IM considered. For example, consider a hypothetical site with M = 7.5, R = 10 km, $Z_{2.5}$ = 1.5 km, fault-type = strike-slip, and V_{s30} = 500 m/s. In Figure 13, the predictability of most of the IMs considered in this study are provided for this hypothetical site using Campbell and Bozorgnia (2008) to calculate $\sigma_{\ln IM|M,R,S}$ for $IM = SA$ and $IM = PGV$, Campbell and Borzorngia (2010) to predict $\sigma_{\ln IM|M,R,S}$ for $IM = CAV$, and Campbell and Bozorgnia (2012) to predict $\sigma_{\ln IM|M,R,S}$ for $IM = AI$. Note that although AI is the most efficient IM, it is, however, for the hypothetical site considered, not the most predictable IM.

The total uncertainty, which considers both the effects of the efficiency and predictability, may be computed according to $\sigma_{\ln EDP|M,R,S} = \left(\sigma^2_{\ln EDP|\ln IM} + b^2\sigma^2_{\ln IM|M,R,S}\right)^{1/2}$, where $\sigma_{\ln EDP|M,R,S}$ represents the total uncertainty and b is the coefficient in the least-squares linear regression equation $\mu_{\ln EDP|\ln IM} = a + b \ln IM$ (e.g., slope in regression lines in Figures 9 and 10), with the assumption that the residuals of $\ln IM|M,R,S$ and $\ln EDP|IM|M,R,S$ are independent. Computation of the total uncertainty for $IM = SA$, PGV, AI, and CAV at the base is provided in Figure 14 with $EDP = DYF$. As seen in Figure 14, the lower predictability in AI (i.e., high $\sigma_{\ln IM|M,R,S}$) results in a total uncertainty that is no longer the lowest for the IMs considered. Now, instead of AI, CAV at the base has the lowest total uncertainty.

The fact that CAV has the lowest total uncertainty suggests that in the common case in which IMs are predicted from a seismic hazard analysis, CAV may be the preferred IM to set the target loading level either probabilistically (e.g., return period of 2,475 years) or deterministically (e.g., 84th percentile). The mean values of the other IMs would then be selected, given (or "conditioned on") the value of CAV as the conditioning intensity measure. In the case in which the IMs at the abutment or toe of the dam are measured directly from a strong ground motion instrument during an earthquake, IM is now known and not predicted (i.e., $\sigma_{\ln IM|M,R,S}$ = 0), and the preferred IM to predict deformation would be the most efficient IM, which in the case of this work is AI. Thus, in the context of predicting damage to a dam following an earthquake in which measured abutment or toe recordings at a dam site are available, AI may be the optimal IM.

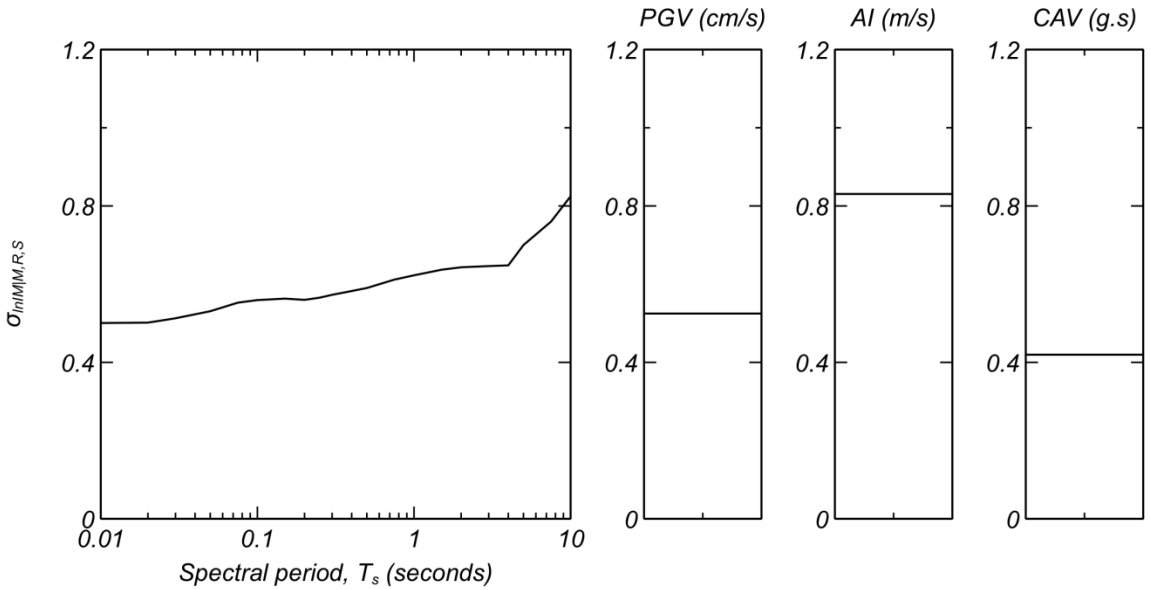

Figure 13: $\sigma_{\ln IM|M,R,S}$ for SA, PGV, AI, and CAV for the hypothetical site considered.

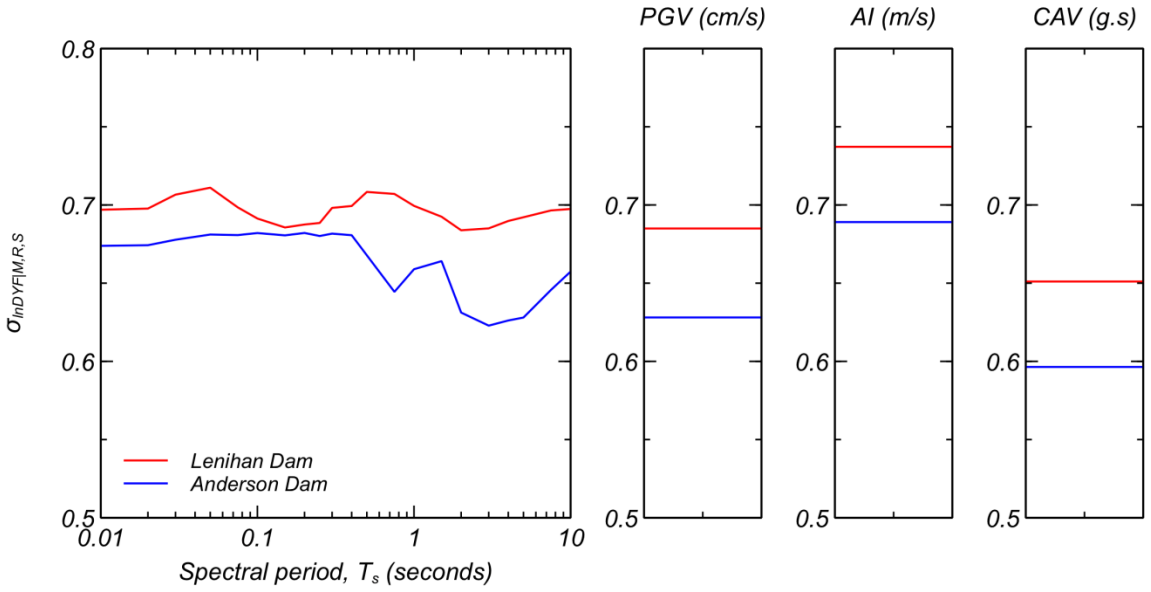

Figure 14: $\sigma_{\ln DYF|M,R,S}$ for SA, PGV, AI, and CAV for the hypothetical site considered.

Conclusions

The measured strong ground motion data at Lenihan and Anderson dams during the 1989 Loma Prieta earthquake provided a useful case-history to assess the capabilities of current NDAs. With the analysis approach described, the NDAs were able to capture reasonably well key dynamic characteristics, such as the surface acceleration response spectra and the magnitude of permanent deformations.

Using the NDA models for both dams, additional analyses with the 342 ground motions provided insight into the relationship between ground motion intensity measures and embankment dam deformation. For the NDA model of the two dams used, AI was the most efficient IM. In terms of SA-based IMs, T_s at short periods and T_s in the general range of the natural period of the dams were seen to be the most efficient SA-based IMs, but were in almost all cases not as efficient as AI. In terms of total standard deviation ($\sigma_{\ln DYF|M,R,S}$) of EDP conditioned on source parameters such as M, R, and S, the poor predictability of AI relative to other IMs resulted in a higher total uncertainty given an earthquake. Within this context, CAV was deemed the best IM.

In conducting a seismic hazard analysis with a dam similar to those modeled, this work suggests that CAV may be the preferred IM to set the target loading level either probabilistically (e.g., return period of 2,475 years) or deterministically (e.g., 84th percentile). In the case in which the IMs at the abutment or toe of the dam are measured directly from a strong ground motion instrument during an earthquake, IM is now known and not predicted (i.e., $\sigma_{\ln IM|M,R,S} = 0$), and the preferred IM to predict deformation would be the most efficient IM, which in the case of this work is AI. Thus, in the context of damage prediction of a dam following an earthquake in which measured abutment or toe recordings at a dam site are available, AI may be the optimal IM.

Acknowledgements

This work was supported by the California Department of Conservation, California Geological Survey, Strong Motion Instrumentation Program, Agreement 1016-988. The funding provided is greatly appreciated.

References

AMEC Geomatrix (2011). Anderson Dam seismic stability evaluation report (SSE-1A), Prepared for Santa Clara Valley Water District.

Ancheta T.D., Darragh R.B., Stewart J.P., Seyhan E., Silva W.J., Chiou B.S., Wooddell K.E., Graves R.W., Kottke A.R., Boore D.M., Kishida T., and Donahue J.L. (2014). NGA-West2 database. *Earthquake Spectra*, 30(3), 989 – 1005.

Armstrong, R.J. (2016). Procedure for selecting and modifying earthquake motions to multiple intensity measures. *Soil Dynamics and Earthquake Engineering*, 89, 91 – 99.

Armstrong, R.J. (2017). Use of the conditional mean for improved prediction of ground motion intensity measures for embankment dams. Proceedings, *2017 Annual United States Society of Dams Conference*.

Armstrong, R.J. (2018a). Cyclic soil behavior of common constitutive models used in non-linear deformation analyses of embankment dams. Proceedings, *2018 Annual United States Society of Dams Conference*.

Armstrong, R.J. (2018b). Numerical analysis of LEAP centrifuge experiments using a practice-based approach. *Soil Dynamics and Earthquake Engineering*., 113, 793 – 803.

Armstrong, R.J. (2018c). Relationship Between Earthquake Ground Motion Intensity Measures and Embankment Dam Deformations. Final Report submitted to California Strong Motion Instrumentation Program, California Geological Survey, Department of Conservation, June 2018.

Beaty, M.H. and Perlea, V.G. (2012). Effect of ground motion characteristics on liquefaction modeling of dams. *ASCE GeoCongress*.

Boulanger ,R. W. and Ziotopoulou, K. (2017). "PM4Sand (version 3.1): A sand plasticity model for earthquake engineering applications." Report No. UCD/CGM-17/01, Center for Geotechnical Modeling, Department of Civil and Environmental Engineering, University of California, Davis, CA, 112 pp.

Bray, J.D. and Travasarou, T. (2007). Simplified procedure for estimating earthquake-induced deviatoric slope displacement. *Journal of Geotechnical and Geoenvironmental Engineering*, 133(4), 381–92.

Byrne, P.M. and Naesgaard, E. (2015). Personal Communications. UDM Version: 5d. https://www.itascacg.com/udms/ubchyst (Accessed 05/30/18).

Campbell, K.W. and Bozorgnia, Y. (2008). NGA ground motion model for the geometric mean horizontal component of PGA, PGV, PGD and 5% damped linear elastic response spectra for periods ranging from 0.01 to 10 s. *Earthquake Spectra*, 24(1), 139-171.

Campbell, K.W. and Bozorgnia, Y. (2010). A ground motion prediction equation for the horizontal component of cumulative absolute velocity (CAV) based on the PEER-NGA strong motion database. *Earthquake Spectra*, 26(3), 634-650.

Campbell, K.W. and Bozorgnia, Y. (2012). A comparison of ground motion prediction equations for Arias intensity and cumulative absolute velocity developed using a consistent database and functional form. *Earthquake Spectra*, 28(3), 931-941.

Chiou, R., Darragh, R., Gregor, N., and Silva, W. (2008). NGA project strong-motion database. *Earthquake Spectra*, 24(1), 23-44.

Cornell, C. A., and Luco, N. (2001). Ground motion intensity measures for structural performance assessment at near-fault sites. *Proc., U.S.– Japan Joint Workshop and Third Grantees Meeting*, U.S.–Japan Cooperative Research on Urban EQ. Disaster Mitigation, Seattle.

Dorsey, C. (2011). Memorandum of design review Leroy Anderson Dam No. 72-9 Santa Clara County. California Division of Safety of Dams.

Itasca Consulting Group. (2016). FLAC, fast lagrangian analysis of continua, user's guide, version 8.0, Itasca Consulting Group, Minneapolis.

Kuhl, J. (2011). Memorandum of design review James J. Lenihan Dam No. 72-8 Santa Clara County. California Division of Safety of Dams.

Ryan, M.J., Mooers, M., Makdisi, F.I., Nelson, J., and Slack, C. (2013). Seismic stability evaluation of Anderson Dam, Santa Clara County, California. Proceedings, *2013 Annual United States Society of Dams Conference*.

Saygili, G. and Rathje, E.M. (2007). Empirical predictive models for earthquake-induced sliding displacements of slopes. *Journal of Geotechnical and Geoenvironmental Engineering*, 134(6), 790–803.

Terra GeoPentech. (2012). Lenihan Dam, site characterization, material properties, and ground motion (Report No. LN-3). Prepared for Santa Clara Valley Water District.